REFLECTANCE SPECTROSCOPY OF DIOGENITE METEORITE TYPES FROM ANTARCTICA AND THEIR RELATIONSHIP TO ASTEROIDS

Lucy A. McFADDEN[1], Michael J. GAFFEY[1], Hiroshi TAKEDA[2], Timothy L. JACKOWSKI[1] and Kevin L. REED[1]

[1]*Planetary Geosciences Division, Hawaii Institute of Geophysics, University of Hawaii, Honolulu, Hawaii 96822, U.S.A.*
[2]*Mineralogical Institute, Faculty of Science, University of Tokyo, 3-1, Hongo 7-chome, Tokyo 113*

Abstract: Spectral reflectance measurements (0.4–2.5 μm) of 3 diogenite meteorites found in Antarctica are examined and compared with previous measurements of diogenites to correlate mineralogy and petrography with the spectral characteristics that can also be measured on solar system objects of unknown composition. The Antarctic diogenites have the same spectral characteristics as other diogenites, however there are measurable differences among all diogenite spectra. Analysis of the spectra into sums of gaussian components reveals bands due to spin-forbidden transitions of Fe^{2+} ions in pyroxene which are identified for the first time in reflectance spectra of powdered samples. From these laboratory measurements it is shown that spectral reflectance measurements of asteroids and other solar system objects made with the visible CVF spectrometer used for laboratory measurements is capable of providing useful information on their surface composition. The absolute calibration of the relationship between pyroxene chemistry and absorption band position of the 0.9 and 2.0 μm bands (ADAMS, J. Geophys. Res., **79**, 4829, 1974) should be recalibrated using new laboratory measurements and for numerically analyzed bands. The trend of the old calibration is not affected. The understanding of the behavior of reflectance spectra of diogenites gained from this study will be used in a future report to analyze the surface composition of the near-earth asteroid 1915 Quetzàlcoatl, which has a diogenite-like reflectance spectrum.

1. Introduction

Meteorites, lunar samples and cosmic dust particles are the only extraterrestrial materials available for study in terrestrial laboratories. Reflectance spectra of meteorites are measured in the laboratory in order to correlate their spectral characteristics with their mineralogy and petrology. Spectral measurements are particularly sensitive to the oxidation state of iron (*e.g.* Fe^{2+}/Fe^{3+}), the presence of other transition elements in minerals, and the mineral structure (*e.g.* clino- *vs.* orthopyroxenes). An understanding of the reflectance spectra of meteorites is essential to interpret reflectance spectra of solar system objects measured with telescope or spacecraft spectrometers. The remote sensing technique of reflectance spectroscopy is presently the only method capable of determining certain aspects of the surface mineralogy and petrology of objects

* PGSD Publ. #352.

from which samples have not been retrieved. The asteroids are a compositionally heterogeneous group of small solar system objects whose nature is known only through remote sensing measurements. For these reasons reflectance spectra of petrologically and petrographically unique meteorites found in the Antarctic meteorite collections are measured.

1.1. Review of spectra of diogenite components

Reflectance spectra of diogenites are dominated by 3 spectral features, a strong absorption band wing in the ultraviolet (UV) region and prominent absorptions located in the 0.9 and 2.0-μm spectral region (Fig. 1). These 3 bands are diagnostic of the presence of pyroxenes in reflectance spectra (*e.g.* ADAMS, 1975). They are the result of metal-oxygen charge transfers in the UV (LOEFFLER *et al.*, 1974) and spin-allowed, Laporte-forbidden transitions of d-orbital electrons (*e.g.* BURNS, 1970) in the near-infrared region. The wavelength positions of the band centers vary as a function of pyroxene chemistry. The absorption band depth and width are functions of pyroxene chemistry, physical state (particle size and texture), temperature and the presence of other mineral components contributing to the spectrum.

1.2. Spin-forbidden bands

Systematic studies of the effects of compositional variation in reflectance spectra of powders (ADAMS, 1974) and in absorption spectra of single pyroxene crystals (HAZEN *et al.*, 1978; GOLDMAN and ROSSMAN, 1979) have previously been made. In single crystal absorption spectra, spin-forbidden crystal field transitions of ferrous iron occur at 0.55, 0.50, 0.460–0.480 and 0.437 μm (HAZEN *et al.*, 1978). Due to their prominence in low iron orthopyroxenes, where the iron preferentially occupies M2 sites these transitions occur within iron cations in M2 sites (GOLDMAN and ROSSMAN, 1979). A band at 0.446 μm is also seen in orthopyroxenes (GOLDMAN and ROSSMAN, 1979) but is not present in the lunar pyroxenes measured by HAZEN *et al.* (1978). Bands at 0.508, 0.488 and 0.468 μm are attributed to Fe^{2+} in the M1 site (GOLDMAN and ROSSMAN, 1979). A band located at the 0.64-μm region is attributed to Cr^{3+} in pyroxenes by HAZEN *et al.* (1978). The results of a study on lunar pyroxenes (BURNS *et al.*, 1976) demonstrated the existence of an absorption band due to titanium in pyroxenes at 0.47 μm. A ferrous iron band is also located in this region in orthoferrosilite and in other pyroxenes.

1.3. Chromite and troilite spectra

Laboratory experiments with the optical absorption spectra of chromites have been carried out by BURNS (1975), MAO and BELL (1975) and STUBICAN and GRESKOVICH (1975). D-orbital transitions in chromium ions in octahedral coordination occur in the vicinity of 0.60 and 0.43 μm. Systematic studies of the variation in absorption parameters with transition element chemistry have not been made. Absorption bands due to Fe^{2+} in chromite are also present at 0.64, 0.66 and 0.68 μm (MAO and BELL, 1975). The spectrum of troilite has not been measured. An iron-sulfide spectrum has been measured and shows a broad, shallow band in the 1.0-μm region (GAFFEY and JACKOWSKI, unpubl.)

1.4. Objectives

We report here the results of a study made on 3 diogenite types found in the

Antarctic collection: Y-74013, Y-75032 and ALH-77256. The samples were provided by the National Institute of Polar Research. The reflectance spectrum of each meteorite is presented and interpreted in terms of its mineralogy and petrology and compared with diogenite spectra previously measured by GAFFEY (1976). The interpretation of the visible region of the spectrum is emphasized because of the application to the interpretation of the spectrum of the near-earth asteroid 1915 Quetzàlcoatl. The uniqueness of the spectral features of each meteorite is discussed and related to the mineralogy and mineral chemistry of the samples.

Gaussian band analysis is used to quantitatively describe the parameters of the absorption bands present in the spectra. Some of the spin-forbidden, relatively weak absorption bands in the visible and UV are resolved with the existing instrumentation but cannot be numerically parameterized.

These bands have not been previously characterized in reflectance spectra of powdered samples. Each spectrum is unique in that some expected bands are absent and/or additional bands are present.

2. Sample Description

2.1. Y-74013

The Y-74013 diogenite is an unbrecciated, recrystallized diogenite with granoblastic texture. Portions of this meteorite consist of transparent orthopyroxene up to 1.0 mm in length. Within the coarse-grained areas are islands of fine-grained darker pyroxene crystals with numerous minute, droplet-shaped inclusions (TAKEDA *et al.*, 1978, 1981). The Yamato diogenites were ground to <37 micron particle sizes.

2.2. Y-75032

The Y-75032 diogenite is an unrecrystallized, monomict breccia. Translucent white pyroxene crystals are set in a dark glassy matrix of pigeonitic composition. The composition of the pyroxenes in this diogenite is the most iron- and calcium-rich among the known meteorites of this type. The pyroxenes have been observed to contain bleby inclusions of augite within the host orthopyroxene which was inverted from pigeonite (TAKEDA *et al.*, 1979).

2.3. ALH-77256

A chip of the Allan Hills diogenite, ALH-77256 was measured consisting of large (mm-sized) clasts with fusion crust on the back side. Veins of fine-grained oxidized material surround the pyroxene clasts and sometimes pass through the clasts in parallel layers. Olivine was not unambiguously identified by microscopic examination of this chip. A few euhedral opaque grains, presumably chromite, are seen. A large clast of clear crystals presumed to be plagioclase because of iridescence on its surface, is approximately 1.0 mm long and located in the center of the sample. A few 0.5 mm plagioclase clasts are also seen elsewhere in the chip. A description of this meteorite also appears in TAKEDA *et al.* (1980).

2.4. Previously measured diogenites

The samples of Johnstown and Tatahouine were ground from a single crystal from each meteorite. Roda and Shalka were alteration and fusion crust-free samples

of crystals and matrix ground to an unknown particle size range (GAFFEY, personal communication). In the absence of petrographic descriptions of the measured samples, we assume that previously published descriptions are representative of the measured samples. This is true of the major element mineralogy (FLORAN *et al.*, 1981), however textural heterogeneity is common in breccias. Mineralogical and petrographic descriptions of these diogenites are reported in MASON (1963). All except Tatahouine are monomict breccias of orthopyroxene dominated mineralogy. Minor amounts of olivine, plagioclase, tridymite, chromite, troilite and metallic iron are present in some but not all samples.

3. Instrumentation

3.1. New measurements

The following description of the instrumentation is adapted from SINGER (1981). Spectral reflectance measurements were made on a spectro-goniometer designed to measure bidirectional reflectance of horizontal samples at adjustable settings of incidence and emission angles. For all measurements reported here, the angle of incidence was 10°, the measured angle of emission was 10°. The light source is a 250 W, 3400 K quartz-halogen bulb placed in a halon-lined integrating enclosure. All optics are reflecting and designed to minimize polarization. The light beam is collimated by an f/8 off-axis parabolic mirror. Spectrometers designed for use at the telescope are mounted onto the goniometer. In the visible and near-infrared region from 0.40–1.00 μm the spectrometer consists of a circular variable filter (CVF) transmitting light with 1.5% wavelength resolution onto a silicon diode detector operated at liquid nitrogen temperature (77 K). A liquid nitrogen-cooled, 1.5% resolution CVF, transmitting light in the 0.60–2.5 μm region onto a liquid nitrogen-cooled indium antimonide detector is used for measurements in the near-infrared spectral region. The reflected light from the sample is directed into one instrument at a time. The signal is chopped by a black blade and the chop signal subtracted from the sample signal in a standard synchronous detection scheme. Scattered light and any differential thermal component not removed by synchronous detection is measured by placing a dark slide in front of the light source. This component is subtracted from the signal by subsequent computer processing.

Measurements of the diffuse reflectance standard called Halon are made periodically throughout an observing period and divided into the measurements of the sample spectrum. Halon, manufactured by Allied Chemical Corporation (VENABLE *et al.*, 1976) consists of 50 μm sized beads of fluorocarbon plastic. A layer of Halon >0.6 cm has an absolute reflectance greater than 99% between 0.4–1.2 μm and greater than 98% between 1.2–2.5 μm. Our spectra are corrected for the small deviations from perfect reflectance of Halon in the near-infrared spectral region in the final stages of computer processing. One of the major advantages of using Halon as a standard is that it does not absorb water.

3.2. Previously published measurements

The diogenites, Johnstown, Roda, Tatahouine and Shalka were previously measured on a Beckman DK-2A ratio recording spectroreflectometer with 0.9% wavelength

resolution at 0.50 μm (GAFFEY, 1976). A MgO-lined integrating sphere was used, resulting in measurements of hemi-spherical reflectance. A photomultiplier tube and leadsulfide detector were used in the visible and near-infrared spectral regions respectively (GAFFEY, 1976).

4. Spectral Analysis

The dark signal and scattered light are subtracted from the measurements which are averaged and divided by the halon measurements in a spectrum processing program (CLARK, 1980) operating on a TI980B computer. We assume that the absorption bands in reflectance spectra are gaussian. However, this analysis technique is continuously evaluated for its applicability to a particular problem. As long as the program can resolve mineralogically meaningful absorption bands with calculated residuals of the same size as experimental error, the technique is adequate for applications of reflectance spectroscopy to planetary objects. Each study in which gaussian analysis is used to describe measured spectra tests this assumption.

The calibrated reflectance spectra are represented by a superposition of gaussian components of the form

$$G(\nu, H, A, \nu_0) = A \exp (\ln 2[2(\nu - \nu_0)/H]^2),$$

using a non-linear least-squares analysis adapted from a program by KAPER *et al.* (1966). Previous studies using this same program include FARR *et al.* (1980), CLARK (1981), SINGER (1981) and McCORD *et al.* (1981).

A solution is determined by minimizing the sum of the squares of the residuals between the observed and calculated representation to a value comparable to the uncertainty in the measurements. The user provides the initial estimates of the gaussian parameters H, A and ν_0, representing full width at half minimum (cm^{-1}), amplitude (%) and position of absorption band minimum (cm^{-1}) respectively. An estimated continuum function is also user-provided which represents that part of the spectrum which is not part of an absorption band. Dividing out a continuum function standardizes the analysis such that parameters can be compared to the same baseline. The equations to satisfy the minimization condition are:

$$\frac{\partial S}{\partial P_1} = \frac{\partial S}{\partial P_2} = \cdots = \frac{\partial S}{\partial P_{3n}} = 0,$$

where p_i represents each variable in a gaussian component. Because gaussian distributions are non-linear, the equations cannot be solved directly. However, they are differentiable with respect to all parameters uniformly, therefore the equations can be linearized by expansion into a Taylor series and solved iteratively. The mathematical solution is however not unique. Independent justification of the reality of the absorption bands is needed to confirm their physical significance.

Analyses of the diogenite spectra were performed initially from estimated parameters based on visual inspection alone. With the knowledge of the mineralogy of the samples, the expected bands were verified. In some instances physically meaningful bands were not included in the initial estimate of bands to be fit. Subsequent

examination of the fitted spectra revealed sinusoidal-shaped residuals across a spectral region corresponding to some of the missing bands. The spectral resolution is not high enough to fit some of these bands as they consist of only 2 or 3 data points. Their presence, albeit uncharacterized, can be observed.

5. Results

5.1. Y-74013

The spectrum of Y-74013 (Fig. 1a) has an albedo of 0.28 at 0.72 μm. The maxi-

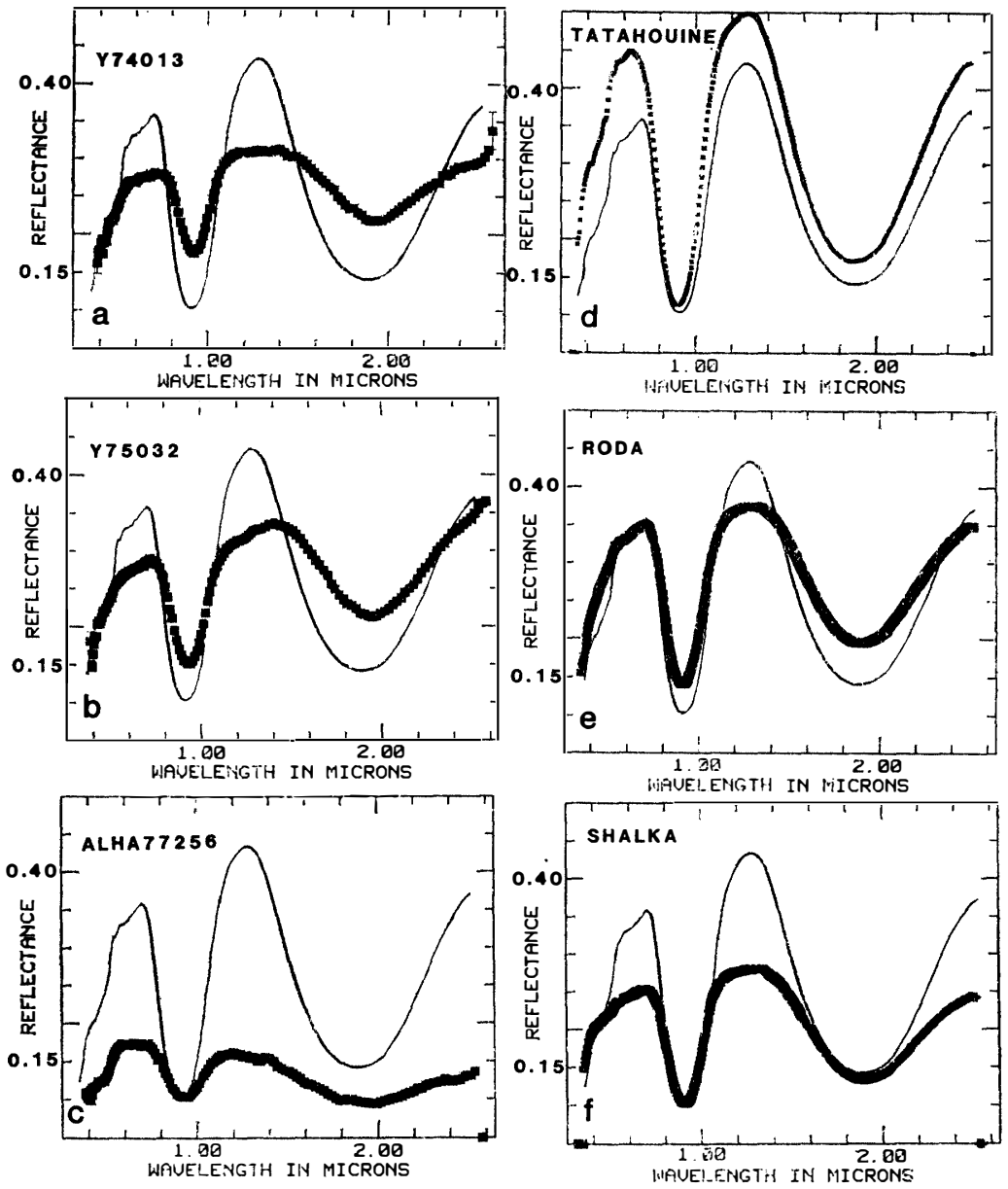

Fig. 1. Reflectance spectra (bold points) of a) Y-74013, b) Y-75032, c) ALH-77256 (whole rock) d) Tatahouine (crushed, single crystal), e) Roda and f) Shalka, compared to spectrum of a crushed, single-crystal of Johnstown (solid line).

mum reflectance between 0.55–0.72 μm forms a gently sloping or even plateau-shaped continuum. The UV absorption band wing and continuum plateau have superimposed weak and narrow bands at 0.70, 0.65, 0.60, 0.50, 0.48 and 0.43 μm (Fig. 2a). The 0.55-μm band is not resolved in this spectrum at this resolution. The 0.9-μm band as fit by gaussian components (Fig. 2b) is composed of two bands centered at 0.895 and 0.962 μm with a band depth of 0.32 and 0.21 relative to unit reflectance respectively.

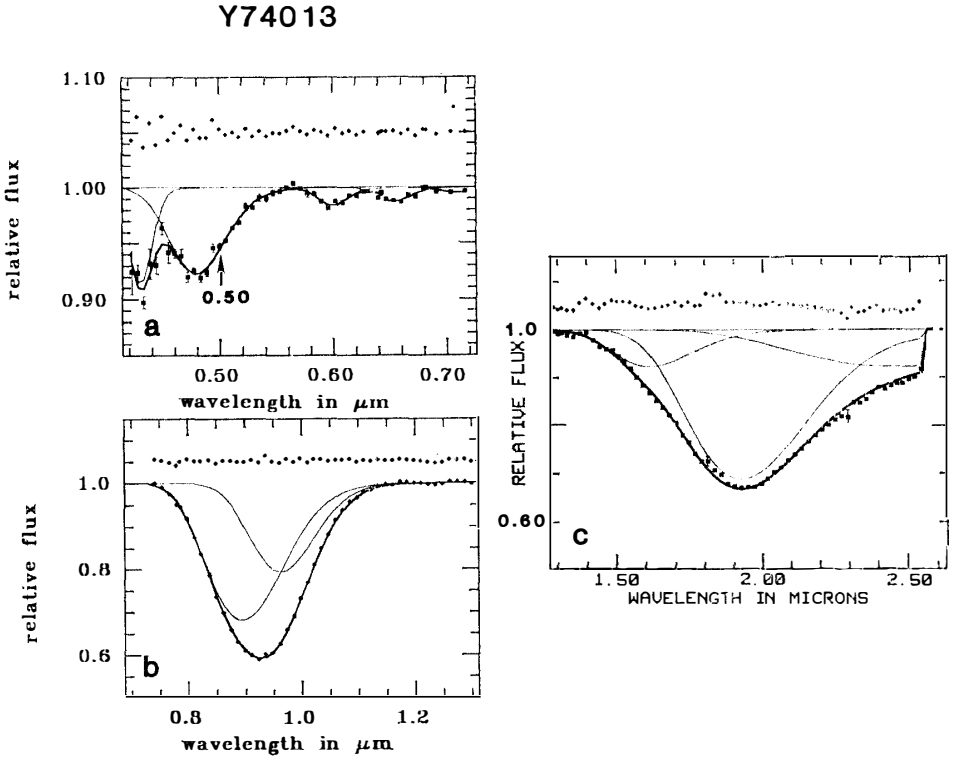

Fig. 2. a) Absorption bands of the visible spectrum of Y-74013 are located at 0.70, 0.65, 0.60, 0.48 and 0.43 μm. The continuum is removed thus the bands are plotted relative to 1.0. The points are the measured spectrum, the bold solid line is the sum of the gaussian components fit to the spectrum. The thinner solid lines are the individual gaussian components. The residuals are plotted relative to 0.05. Note these figures are plotted to enhance the existence of the bands, therefore the vertical scales vary. b) Same as (a) for the 0.9-μm pyroxene band. Absorption bands are resolved at 0.89 and 0.96 μm. c) Same as (a) for the 2.0-μm pyroxene band.

The bandwidths are 0.18 and 0.14 μm. The albedo at 1.30 μm between the 0.9 and 2.0-μm bands is 0.31. There is a weak inflection at 1.23 and 1.43 μm (Fig. 1a). Again the continuum is plateau-shaped in this spectral region instead of peaked. The 2.0-μm band is a composite band which cannot be completely characterized due to the long wavelength limit of the data. Figure 2c shows that 3 gaussian bands can be resolved.

5.2. Y-75032

The spectrum of Y-75032 (Fig. 1b) has an albedo of 0.287 at 0.72 μm. A weak absorption band is seen at 0.625 μm (Fig. 2d). A strong UV absorption band wing has superimposed weak and narrow bands at 0.50 and 0.43 μm (Fig. 2d) which cannot

be characterized as gaussian components with the existing spectral resolution. The 0.47 and 0.55-μm ferrous iron bands are missing. The 0.9-μm region is composed of 3 gaussian absorption bands located at 0.900, 0.966 and 1.185 μm (Fig. 2e). The relative band depths are 0.422, 0.231 and 0.046 respectively. The bandwidths are 0.21, 0.15 and 0.14 respectively. The continuum between the 0.9 and 2.0-μm band peaks at 1.40 μm at an albedo of 0.33. There is a distinct continuum maximum in this region of this spectrum as in the visible. The 2.0-μm band is a composite of 2 gaussian functions (Fig. 2f).

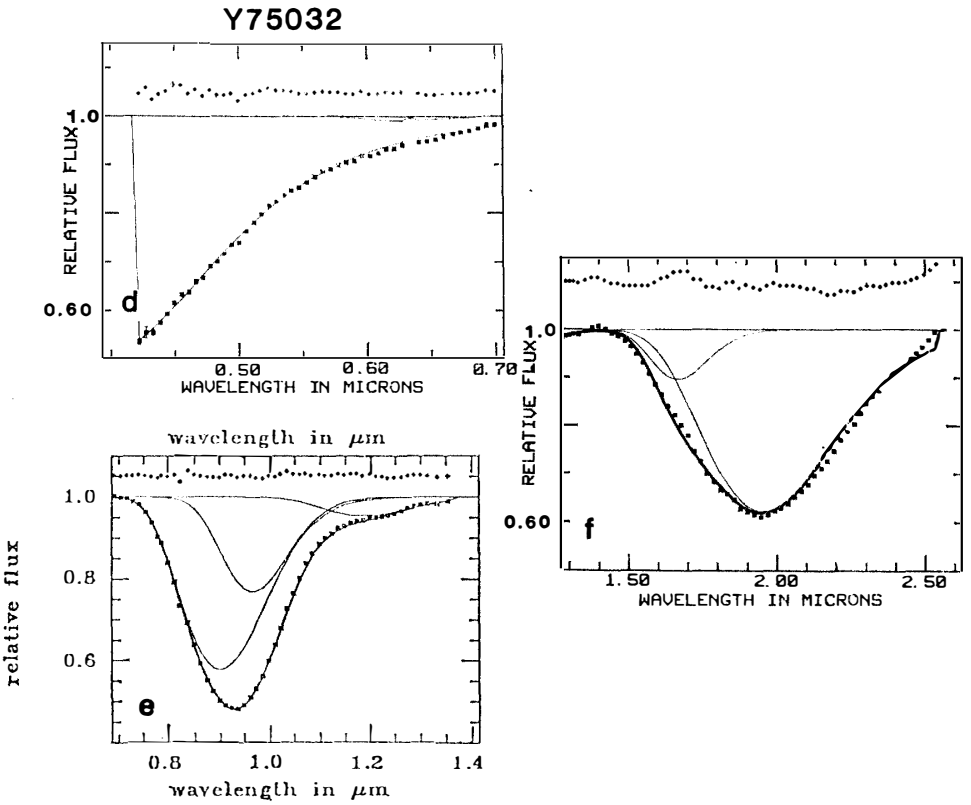

Fig. 2. d) same as (a) for Y-75032 visible spectrum. The 0.50-μm band cannot be fit but can be detected as a negative residual. e) Two pyroxene bands and 1 plagioclase band are resolved in the 0.9-μm region spectrum of Y-75032. f) The 2.0-μm region of Y-75032.

5.3. ALH-77256

ALH-77256 has a spectrum (Fig. 1c) with a plateau-shaped continuum in the visible region between 0.56 and 0.72 μm with weak and narrow superimposed absorption bands at 0.67 and 0.62 μm (Fig. 2g). The spectrum of ALH-77256 has bands at 0.48 and 0.43 μm (Fig. 2g). The 0.9-μm band is composed of 2 or 3 absorption bands which are difficult to mathematically express as sums of gaussian bands evidenced by the large residuals in Fig. 2h. The continuum reflectance beyond the 0.9-μm band is lower than the visible maximum reflectance (Fig. 1c). The near-infrared albedo reaches a maximum of 0.16. There are narrow absorption bands superimposed on the

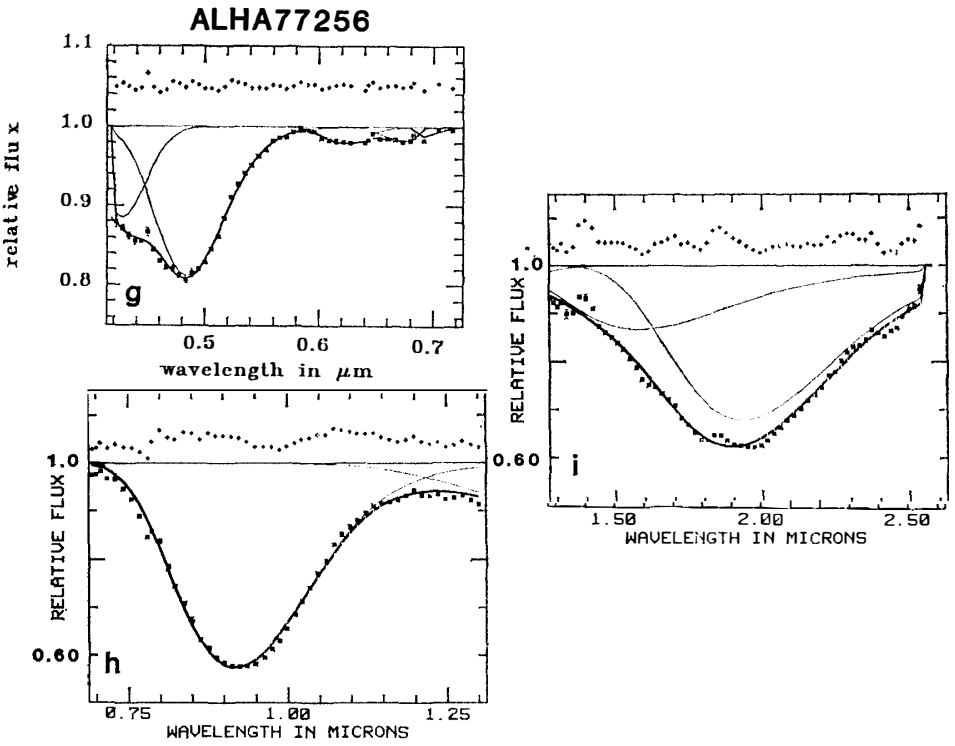

Fig. 2. g) The visible region gaussian fitted spectrum of ALH-77256. Absorption bands are resolved at 0.67, 0.62, 0.48 and 0.43 μm. h) 0.9-μm region of ALH-77256. i) The 2.0-μm region of ALH-77256.

2.0-μm band (Fig. 2i). The 2.0-μm band dominates the near-infrared region yet the continuum remains low at the infrared end of the absorption band.

6. Interpretation

The spectra will be initially interpreted based on existing calibrations and interpretive techniques as referenced. Any unreferenced interpretations are derived from this study and will be discussed in the following section.

6.1. Y-74013

The 0.50, 0.48 and 0.43-μm bands (Fig. 2a) are due to spin-forbidden transitions of electrons in Fe^{2+} cations in pyroxene (HAZEN *et al.*, 1978). The band at 0.60 μm is due to Cr^{3+} in pyroxene. The band at 0.65 is assigned to Ti^{3+} or Cr^{3+} in chromite (MAO and BELL, 1975). The 0.70-μm band is cannot be unambiguously assigned. It may be a chromium band in chromite (MAO and BELL, 1975). The composite 0.9-μm band (Fig. 2b) has a band center at 0.924 μm indicating an average pyroxene composition with about 72% Fe/(Mg+Fe+Ca) and 8% Ca/(Mg+Fe+Ca) (ADAMS, 1974) (Fig. 3). The 0.89-μm band (Fig. 2b) is a spin-allowed Fe^{2+} transition in the highly distorted M2 site in orthopyroxene (BURNS, 1970). There are 6 possible assignments of the 0.966-μm band. The possibilities will be presented here and discussed in the next section. The band may be due to (1) a spin-allowed transition in a high Fe pigeonite,

(2) an absorption in troilite (GAFFEY and JACKOWSKI, unpublished), (3) a spin-allowed Fe^{2+} transition in the M1 site in orthopyroxene, (4) a glass band, (5) a polarization component, and (6) a mathematical artifact. The 2.0-μm band arises from spin-allowed electronic transitions of ferrous iron in the M2 site in orthopyroxenes (GOLDMAN and ROSSMAN, 1979). Either the 2.0-μm band is not gaussian and/or additional components are present. Compared to spectra of pure pyroxenes (SINGER, 1981) the albedo of Y-74013 is at least 50% less than that of a pure pyroxene of equivalent particle size. There is an absorbing component that reduces the albedo. In this case dispersed opaque material acts as an absorbing medium and reduces the albedo at all wavelengths. The assignment of the 1.23-μm band is presently unknown.

6.2. Y-75032

The visible absorption bands in the spectrum of Y-75032 have the same interpretation as those in Y-74013 except that some of the bands are missing. The 0.39-μm band is probably an oxygen→metal charge transfer band (LOEFFLER *et al.*, 1974). The composite 0.9-μm band has the same characteristics as that of Y-74013 and will be discussed in the next section. The band at 1.185 μm is attributed to Fe^{2+} in octahedral coordination sites in plagioclase (ADAMS and GOULLAUD, 1978). An absorbing component has reduced the albedo of this sample. There is no indication of the nature of this absorbing material from examination of the reflectance spectrum alone. From independent petrographic studies (TAKEDA *et al.*, 1979) a glassy matrix and blebby inclusions of augite are known to be present. A significant glass component can lower the overall albedo of a spectrum (*e.g.* ADAMS, 1975) as can the presence of blebby augite inclusions. The plateau-shaped continuum seen in the spectrum of Y-74013 is not present due to the presence of the band at 0.62 μm and the plagioclase absorption band at 1.18 μm.

6.3. ALH-77256

The spin-forbidden iron bands in the visible are not present in the whole rock spectrum of ALH-77256 (Fig. 2g). The 0.50-μm band is masked by the strong band at 0.48 μm. The 0.55-μm band is not resolved with the instrumentation used. The relatively strong 0.48-μm band is most likely an Fe^{3+} absorption (BURNS and VAUGHAN, 1975). This assignment is made based on its strength relative to other bands in the same position in other diogenite spectra and the observed iron oxide in the ALH-77256 sample. The 0.62-μm band is due to chromium in pyroxene. The 0.67-μm band may be due to Fe^{3+} from terrestrial weathering or Cr^{3+} in chromite (MAO and BELL, 1975). The pyroxene bands in ALH-77256 are broader than those in the spectrum of Y-74013 and Y-75032. One band can be poorly fit to the 0.9-μm absorption (Fig. 2h). The large grain size of the orthopyroxene clasts provides a very long optical path length resulting in high absorption at all wavelengths but more absorption in the regions of interelectronic transitions. It is likely that the optical beam penetrated through the clasts and was absorbed by the fusion crust on the back of the chip. Some of the structure in the 2.0-μm region may be water bands from fluid inclusions that have recently been reported (ASHWAL *et al.*, 1981; BERGMAN *et al.*, 1982). The overall negative slope of the near-infrared portion of the curve is commonly seen in spectral reflectance measurements of whole rock specimens (SINGER and BLAKE, 1982). It is im-

portant to make measurements of a powdered sample of this meteorite with the fusion crust removed. If the features in the 2.0-μm region are still present without any fusion crust, then the features can be attributed to the fluid inclusions or other mineral/chemical species.

7. Comparisons and Discussion

7.1. Johnstown spectrum compared to other diogenite spectra

The albedo of Johnstown is 20% higher than that of the Yamato diogenites at 0.70 μm and twice as bright as the Allan Hills diogenite at this wavelength (Figs. 1a–1c). The albedo and spectral contrast of whole rock spectra is always lower than spectra of powdered samples due to the reduced number of grain boundaries. The difference in albedo between Tatahouine and Johnstown (Fig. 1d) can be attributed to particle size. The Tatahouine sample consists of smaller particle sizes than Johnstown and therefore has a higher reflectance. The difference in albedo between Johnstown and the Yamato diogenites (Figs. 1a–1b), Roda (Fig. 1e) and Shalka (Fig. 1f), cannot be attributed to particle size alone. With an increase in particle size, the continuum reflectance has been shown to decrease (ADAMS and FILICE, 1967). The continuum reflectance of the smaller particle-sized Yamato diogenites is lower than the larger particle-sized, Johnstown and Tatahouine diogenites. Therefore the particle size does not control the albedo of the spectra in this case. The matrix components of Y-75032 and Shalka contain absorbing material that lowers the albedo of the continuum. The dusty opaques in the recrystallized diogenite, Y-74013, cause its continuum to be low in albedo.

7.2. Band strengths

The major pyroxene bands in the previously measured spectra of diogenites (GAFFEY, 1976) are approximately 50% stronger compared to the Yamato diogenites (Fig. 1). ALH-77256 has a comparably low reflectance in the center of the 0.9-μm band and the reflectance in the 2.0-μm band is lower than that of Johnstown, because of large grains in the single particle (chip). The Johnstown and Tatahouine diogenites were crushed from a single crystal, therefore each particle, which is larger than the particle size of Y-74013 and Y-75032, consists of a single grain, and more photons are absorbed than reflected off grain boundaries. Thus the absorption bands are deeper. With many grains per particle, more photons are reflected from grain boundaries and the reflectance in the absorption band is higher. The <37-μm particle size of the Antarctic samples is below the size for maximum spectral contrast (KING *et al.*, 1981). Specular reflections off many particle boundaries should result in a high albedo and low spectral contrast. Their albedo is apparently reduced by the dark troilite inclusions (Y-74013) and glass (Y-75032) well-mixed in the crushing process.

7.3. Comparisons of continua of Yamato diogenites

While the spectra of Y-74013 and Y-75032 are noticeably different due to their respectively flat and peaked continua in both the visible and near-infrared, there is no explanation in terms of optical interactions which can be correlated with the textural differences of these two diogenites. Instead, the differences appear to be mineralogi-

cally controlled. The 0.625-μm band and the plagioclase band at 1.18 μm in the spectrum of Y-75032 absorb preferentially over the component which lowers the continuum.

7.4. The 0.9-μm absorption bands

The possible explanations of the gaussian-fit 0.96-μm band result in no definite conclusion. The possibilities are discussed in the order they were presented.

7.4.1. A spin-allowed transition in a high Fe clinopyroxene

Y-74013 does not contain any clinopyroxene (TAKEDA *et al.*, 1981). The spectrum of Y-75032 contains two 0.9-μm bands consistent with the presence of blebby inclusions of augite in host orthopyroxene (TAKEDA *et al.*, 1979). The band does have physical significance for Y-75032, but not Y-74013. This is not a very convincing case for the physical significance of the band since its presence can be explained in one sample but not the other.

7.4.2. An absorption in troilite

GAFFEY and JACKOWSKI (unpublished) have measured a spectrum of iron sulfide. It has a broad, shallow absorption band in the 1.0-μm region. It is unlikely that this is the cause of the 0.966-μm band such a band would be relatively stronger in the spectrum of Y-74013 than in Y-75032 due to the higher abundance of troilite in Y-74013. The characteristics of the two 0.966-μm bands are similiar.

7.4.3. A spin-allowed transition in the M1 orthopyroxene site

GOLDMAN and ROSSMAN (1979) conducted experiments showing the position of absorptions due to iron in the M1 sites in orthopyroxene. Such absorptions are centered at 0.769 and 1.16 μm in orthopyroxenes. The 0.966-μm band is not at the same wavelength as an M1 site transition. M1 site absorptions observed in pyroxenes of Fs_{14} (Bamle), $Fs_{29.5}$ (Gore Mountain) and Fs_{86} (Manchuria) all show M1 site absorptions at 1.13 μm (GOLDMAN and ROSSMAN, 1979; BURNS, 1970). The position of this band does not shift with increasing iron content. Therefore, the 0.966-μm band is not due to iron in pyroxene in the M1 site.

7.4.4. A glass band

Glass bands are broader than the 0.966-μm band and usually centered at lower energy (FARR *et al.*, 1980). Therefore, it is unlikely that it is a glass band.

7.4.5. A polarization component

The optical design of the spectrometer is such that polarized components cancel. It is possible that there remains a polarized component. However, instrumental tests must be made to provide independent evidence for or against this hypothesis.

7.4.6. A mathematical artifact

KAPER *et al.* (1966) discuss the nonuniqueness of the solutions of a least squares analysis of gaussian components. However, a single gaussian band cannot be fit to these spectra in the 0.9-μm region. Therefore, there is more than one 0.9-μm spectrally active component in this meteorite or the assumption that the band is gaussian is invalid. It is entirely possible, even probable that with the high S/N spectra of laboratory samples that the band profiles are not gaussian. Data from the telescope however, can be fit to gaussian absorptions (P. LUCEY, personal communication). The fact that diogenites are not pure pyroxenes may also factor into the cause of the non-gaussian behavior. Rock assemblages may not be represented by gaussian components

due to the contribution of material which cannot be represented by gaussians.

7.5. Visible absorption bands and minor element mineralogy

Table 1 lists the observed absorption bands in the visible region of the spectrum and code letter or number referring to their spectral characteristics in each specrtum. It is clear that not all of the spin-forbidden Fe^{2+} bands are present in all diogenite spectra. In addition the band parameters vary. Additional non-Fe^{2+} spin-forbidden bands in the visible spectral region are sometimes present. They may be due to additional cations in pyroxenes, or they may be due to transition elements in other mineral components such as chromite or troilite. A consideration of the various cations in pyroxenes and the nature of their spectral contribution will be made.

Table 1. Visible absorption band characteristics[1].

λ	Y-74013	Y-75032	ALH-77256	Johnstown	Tatahouine	Roda	Shalka
0.33	a	a	a	.6	a	a	s
0.392	a	0.384	a	a	a	a	a
0.43	0.086	0.285	0.114	.6	s	pw	a
0.446	a	pw	pw	a	a	a	a
0.481	0.077	pw	0.188	a	p	a	a
0.506	0.039	pw	a	0.069	ps	p	pw
0.548	a	pw	a	p	p	p	pw
0.60	0.016	a	a	.12	p	p	p
0.622	a	a	0.020	a	a	a	a
0.65	0.012	a	a	a	a	a	a
0.675	a	a	0.017w	a	a	a	a
0.70	0.005	a		a	a	a	a

1) 1.0–Exp (depth)
a=absent, p=present, w=weak, s=strong.

7.5.1. Absence of Fe^{3+}

A band located at 0.60 μm has been attributed to Fe^{3+} in terrestrial pyroxenes (BURNS *et al.*, 1976). It is unlikely that there is any endogenic Fe^{3+} in diogenitic pyroxenes because the absence of magnetite in all and the presence of metallic iron in some diogenites (GOOLEY and MOORE, 1976) indicates a relatively high state of reduction. Therefore absorption bands in the 0.60-μm region are not ferric iron bands.

7.5.2. Chromium

All spectra have a band between 0.60–0.62 μm attributed to chromium in pyroxene. Diogenitic pyroxenes are notably high in chromium (Table 2) and the presence of this band is a diogenite indicator. This assignment is chosen from the knowledge that lunar pyroxene bands have a chromium band at 0.64 μm (HAZEN *et al.*, 1978), that Cr^{3+} signatures of some silicates are located between 0.55–0.58 μm (PARKIN and BURNS, 1980), and that the Johnstown diogenite containing 0.78–0.81% by weight Cr_2O_3 in its pyroxene (FLORAN *et al.*, 1981) has an absorption band in its spectrum at 0.60 μm and not at longer wavelengths.

The chemical variations of transition element oxides and Al_2O_3 of chromites are listed in Table 2. If chromite contributes to the spectrum of diogenites, the higher titanium content of the chromite in Y-75032 should be observable in its spectrum.

Table 2. Transition element and Ca and Al oxide content in diogenite pyroxenes and chromites.

Pyroxenes	Y-74013[1]	Y-75032[2]	ALH-77256[3]	Johnstown[4]	Tatahouine[4]	Roda[4]	Shalka[4]
TiO_2	0.03–0.23[a]	0.18–0.38	0.16–0.19	0–0.21	<0.1	<0.1–0.25	<0.1
Cr_2O_3	0.81–1.24	0.22–0.44	0.24–0.37	0.78–0.81	0.70	0.50–0.76	0.40
FeO	14.86–16.52	19.47–21.35	15.13–15.28	15.5–15.6	15.6	15.6–15.7	16.4
MnO	0.55–0.67	0.61–9.76	0.26–0.57	0–0.50	0.52	0–0.57	0.64
CaO	1.12–1.53	1.16–2.72[b]	0.82–1.16	1.39–1.48	0.77	1.36–1.45	0.79
Chromites							
TiO_2	0.69	2.28	0.87	—	—	1.11–2.33	0.59
Cr_2O_3	59.8	53.9	43.4	—	—	50.3	59.0
FeO	24.3	31.9	25.8	—	—	30.1	28.5
MnO	0.54	0.62	0.66	—	—	nd	0.77
Al_2O_3	7.30	7.14	21.4	—	—	9.35–12.9	6.67

1. TAKEDA *et al.*, 1981, 2. TAKEDA *et al.*, 1979, 3. TAKEDA, 1979, 4. FREDRIKSSON *et al.*, 1976,
a. TAKEDA *et al.*, 1978, b. Augite blebs have 22.36% CaO.
— Omitted due to absence of chromite in samples used for reflectance spectroscopy.

The 0.39-μm band in Y-75032 has the depth and appropriate position for a charge transfer band, possibly a metal→metal transition (LOEFFLER *et al.*, 1974). The high aluminum content of chromite in ALH-77256 is notable but without a spectrum of controlled particle size, no conclusion can be made concerning a possible chromite signature in this meteorite. Not all of the bands reported in laboratory spectra of chromites are seen. Systematic studies of chromite spectra need to be made to confirm the assignments of the suggested chromite bands and explain the absence of other expected bands.

7.5.3. Titanium and manganese

The TiO_2 content of measured Y-74013 pyroxenes is 0.23% (TAKEDA *et al.*, 1978) which is the highest TiO_2 content in any of the diogenites with measured reflectance spectra (Table 2). The band at 0.65 μm is present only in the spectrum of Y-74013 and is therefore likely to be caused by titanium. Because the MnO content varies between 0.5–0.6% in diogenitic pyroxenes, its signature, if present, should be seen in all samples. It is not, and is therefore not present in spectrally detectable amounts.

7.6. Major element pyroxene compositions

The observed difference in the iron abundance in the pyroxenes of Y-74013 and Y-75032 from microprobe measurements (TAKEDA *et al.*, 1978, 1979, 1981) is not detectable in these reflectance spectra. This was determined by comparing the predicted shift in band position (ADAMS, 1974) to the wavelength resolution of the measurements. The chemistry difference corresponds to a shift of 0.007 μm at 0.90 μm.

7.7. Plagioclase

The presence of spectrally detectable plagioclase in Y-75032 diogenite spectrum is a distinguishing characteristic of this meteorite. Spectra of eucrites which are pyroxene and plagioclase assemblages have 0.9-μm absorption bands centered at longer wavelengths consistent with their higher iron and calcium pyroxene chemistry (MCFADDEN *et al.*, 1981). Therefore this diogenite type which is an intermediate composition between common diogenites and eucrites (TAKEDA and MORI, 1981), can be identi-

fied from reflectance spectra by the low iron, low calcium pyroxene bands and the plagioclase band.

7.8. Calcium

The spectra were examined for correlations of spectral features with calcium content on the grounds that calcium severely alters the pyroxene crystal structure. There may be a correlation between calcium content and the slope of the UV absorption at wavelengths below 0.50 μm The slope of the UV absorption increases with increasing calcium content. It is clear that particle and grain size also contribute to the slope. Further experiments with controlled particle sizes need to be made to confirm this observation.

7.9. Pyroxene calibration

The calibration of the pyroxene composition and absorption band positions of ADAMS (1974) (Fig. 3) is applicable for composite absorption bands representing average pyroxene composition. A separate calibration for gaussian resolved absorption bands must be determined. The major element chemistry of the pyroxenes as determined from the position of the composite 0.9-μm band and the pyroxene calibration as determined by ADAMS (1974) does not agree with microprobe measurements of iron and calcium in the Antarctic diogenites (TAKEDA *et al.*, 1978, 1979; TAKEDA, 1979). Low calcium, low iron pyroxenes of these diogenites have higher energy absorption bands than clinopyroxenes, consistent with ADAMS' calibration; however the absolute calibration is not accurate. When the pyroxene calibration (ADAMS, 1974) was developed, the band positions were visually read off an analog plot of the reflectance curve (ADAMS, personal communication). The band minimum was assumed to be the band center, an assumption which is valid only in the absence of a continuum slope and when the band consists of a single component. With the introduction of gaussian band analysis (FARR *et al.*,

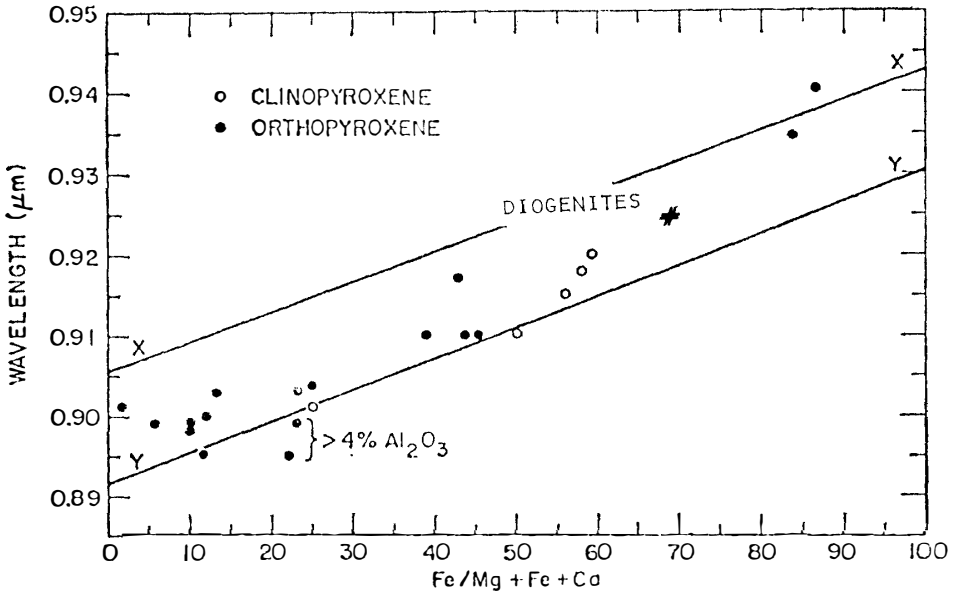

Fig. 3. The relationship of band position to pyroxene iron chemistry as calibrated by ADAMS (1974) for orthopyroxenes and low-calcium clinopyroxenes.

1980; McCord *et al.*, 1981) and the resulting quantification of band parameters, it is possible to resolve more than one absorption in a region of the spectrum which was previously considered to be one. It is therefore possible, if more than one band is present, to determine more than the average pyroxene composition. However, Adams' (1974) pyroxene calibration can only be used as a qualitative indicator of the pyroxene composition. A new calibration will be derived in a future project. Another pyroxene calibration derived in the initial survey of meteorite spectra (Gaffey, 1976) also shows a shift in absolute calibration relative to that of Adams'. Caution should be exercised in using calibration-compatible techniques for determining pyroxene chemistry from band positions. As discussed previously, it is also important to account for the possible non-uniqueness of any particular band.

7.10. Usefulness of the visible CVF spectrometer at the telescope

The near-infrared sensitive spectrometer is used at a 2.2 m telescope for objects as faint as 11.0th magnitude with a S/N ratio of 5 in 5 minutes of integration time. This is one of the most sensitive instruments available at this wavelength resolution. The visible spectrometer has not been extensively used at the telescope to date, primarily because of the recent advancement in infrared detector technology and interest in the relatively unexplored near-infrared spectral region. The standard visible photometer used for faint object measurements has 5% resolution at 0.50 μm. The spectra presented here are evidence of the usefulness of the visible CVF spectrometer for asteroid and other solar system spectral reflectance measurements.

7.11. Application to asteroid surface composition

Figure 4 shows a reflectance spectrum of the asteroid 4 Vesta measured at NASA's Infrared Telescope Facility (IRTF), Mauna Kea, Hawaii (Gaffey, in preparation). The measurements were made with the near-infrared CVF spectrometer used to measure laboratory spectra reported here. Variations of band parameters can be seen over the surface of Vesta as it rotates corresponding to large scale variations in its surface composition (Gaffey, 1981). The knowledge obtained from laboratory spectra of basaltic achondrites is directly applicable to determining the surface composition and thus part of the history of the asteroid.

Another basaltic achondrite-like assemblage has been recently discovered in the near-earth asteroid population (McFadden, 1981). 1915 Quetzàlcoatl has a measured

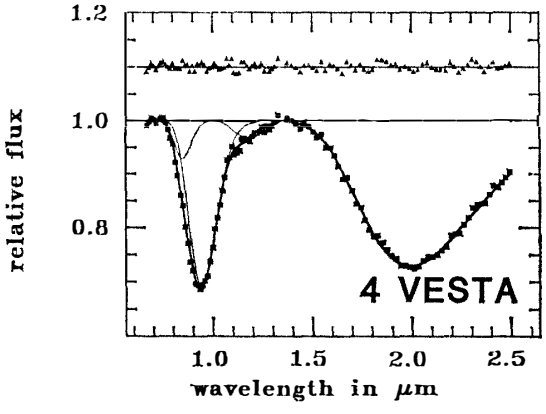

Fig. 4. A reflectance spectrum of asteroid 4 Vesta. At this rotational phase, two pyroxene bands and a plagioclase band are resolved in the 0.9-μm spectral region.

reflectance spectrum of a diogenite-like assemblage. The understanding of the diogenite spectra gained from the results presented here will be applied toward determining the relationship of 1915 Quetzàlcoatl to the diogenites and the basaltic achondrite parent body in a subsequent paper.

8. Summary

Reflectance spectra of Antarctic diogenites are dominated by the major absorption bands characteristic of low-calcium, low-iron orthopyroxenes. These features and an absorption at 0.60–0.62 μm due to Cr^{3+} in pyroxene are diagnostic of diogenite assemblages. The spectrum of Y-74013 is different from those of other diogenites in that the continuum is plateau-shaped. The mechanism causing this shape is not completely understood. From mineralogical and petrographical investigations it seems that only minute, dispersed opaque grains can be suppressing the reflectance outside of the pyroxene bands (Takeda *et al.*, 1981). Unfortunately, there is no obvious spectral signature of the granoblastic texture which makes this diogenite unique. Prior to measuring the reflectance spectrum of Y-75032, a solar system object with such a spectrum would have been classified as a eucrite due to the significant contribution of plagioclase to the reflectance spectrum. However, the position of the orthopyroxene band clearly places this meteorite in the diogenite field.

The ALH-77256 diogenite was measured as a whole rock specimen. The spectrum has the characteristic low albedo and low spectral contrast of an uncrushed sample. The diogenite signature is present nevertheless. Additionally there are narrow, weak absorption bands present which are not seen in other spectra of diogenites. A search for fluid inclusions of water can be made after gaussian band analysis of the 2.0-μm region is performed.

An adjustment to the absolute calibration of the pyroxene band position as a function of pyroxene chemistry (ADAMS, 1974) has been shown to be necessary due to the technique of expressing absorption bands as sums of gaussian bands. The trend of the relationship of band position relative to pyroxene chemistry established previously (ADAMS, 1974; HAZEN *et al.*, 1978) is not affected by the band analysis technique.

The spin-forbidden Fe^{2+} bands in pyroxenes are observed for the first time in powdered samples measured in reflected light. The presence of these bands indicates that the use of the visible CVF spectrometer at the telescope will be useful for mineralogical studies of the surface composition of solar system objects.

Acknowledgments

We would like to thank the National Institute of Polar Research for supplying the meteorite samples. This research was supported with funds from NASA grant NSG 7462. We appreciate the helpful reviews by and discussions with Pamela BLAKE, Paul LUCEY, Roger CLARK, Robert SINGER and 2 anonymous reviewers.

References

ADAMS, J. B. (1974): Visible and near infrared diffuse reflectance spectra of pyroxenes as applied to remote sensing of solid objects in the solar system. J. Geophys. Res., **79**, 4829–4836.

ADAMS, J. B. (1975): Interpretation of visible and near-infrared spectra of pyroxenes and other rock-forming minerals. Infrared and Raman Spectroscopy of Lunar and Terrestrial Minerals, ed. by C. KARR. New York, Academic Press, 90–116.

ADAMS, J. B. and FILICE, A. L. (1967): Spectral reflectance 0.4 to 2.0 microns of silicate rock powders. J. Geophys. Res., **72**, 5705–5715.

ADAMS, J. B. and GOULLAUD, L. H. (1978): Plagioclase feldspars: Visible and near-infrared diffuse reflectance spectra as applied to remote sensing. Proc. Lunar Planet. Sci. Conf. 9th, 2901–2909.

ASHWAL, L. D., BERGMAN, S. C., GIBSON, E. K., HENRY, D. J., LEE-BERMAN, R., MOGK, D. W. and WARNER, J. L. (1981): Liquidvapor inclusions in achondritic meteorites. Meteoritics, **16**, 290.

BERGMAN, S. C., WARNER, J. L., HENRY, D. J., ASHWAL, L. D., LEE-BERMAN, R. and GIBSON, E. K. (1982): Fluid inclusions in diogenite ALHA-77256. Lunar and Planetary Science XIII. Houston, Lunar Planet. Inst., 35–36.

BURNS, R. G. (1970): Mineralogical applications of crystal field theory. London, Cambridge Univ. Press, 255 p.

BURNS, R. G. (1975): Crystal field effects in chromium and its partitioning in the mantle. Geochim. Cosmochim. Acta, **39**, 857–864.

BURNS, R. G. and VAUGHAN, D. J. (1975): Polarized electronic spectra. Infrared and Raman Spectroscopy of Lunar and Terrestrial Minerals, ed. by C. KARR. New York, Academic Press, 39–72.

BURNS, R. G., PARKIN, K. M., LOEFFLER, B. M., LEUNG, I. S. and ABU-EID, R. M. (1976): Further characterization of spectral features attributable to titanium on the moon. Proc. Lunar Sci. Conf. 7th, 2561–2578.

CLARK, R. N. (1980): A large scale interactive one dimensional array processing system. Publ. Astron. Soc. Pac., **92**, 221–224.

CLARK, R. N. (1981): Water frost and ice: The near-infrared spectral reflectance 0.65–2.5 μm. J. Geophys. Res., **86**, 3087–3096.

FARR, T. G., BATES, R. L., RALPH, R. L. and ADAMS, J. B. (1980): Effects of overlapping optical absorption bands of pyroxene and glass on the reflectance spectra of lunar soil. Proc. Lunar Planet. Sci. Conf. 11th, 719–729.

FLORAN, R. J., PRINZ, M., HLAVA, P. F., KEIL, K., SPETTEL, B. and WANKE, H. (1981): Mineralogy, petrology and trace element geochemistry of the Johnstown meteorite: A brecciated orthopyroxenite with siderophile and REE-rich components. Geochim. Cosmochim. Acta., **45**, 2385–2391.

FREDRIKSSON, K., NOONAN, A. and BRENNER, P. (1976): Bulk and major phase composition of eight hypersthene achondrites. Meteoritics, **11**, 278–280.

GAFFEY, M. J. (1976): Spectral reflectance characteristics of the meteorite classes. J. Geophys. Res., **81**, 905–920.

GAFFEY, M. J. (1981): Surface material variegation on asteroids. Bull. Am. Astron. Soc., **13** (3), 711.

GOLDMAN, D. S. and ROSSMAN, G. R. (1979): Determination of quantitative cation distribution in orthopyroxenes from electronic absorption spectra. Phys. Chem. Minerals, **4**, 43–53.

GOOLEY, R. and MOORE, C. B. (1976): Native metal in diogenite meteorites. Am. Mineral., **61**, 373–378.

HAZEN, R. M., BELL, P. M. and MAO, H. K. (1978): Effects of compositional variation on absorption spectra of lunar pyroxenes. Proc. Lunar Planet. Sci. Conf. 9th, 2919–2934.

KAPER, H. G., SMITS, D. W., SCHWARZ, U., TAKAKUBO, K. and VAN WOERDEN, H. (1966): Computer analysis of observed distributions into gaussian components. Bull. Astron. Inst. Neth., **18**, 465–487.

KING, T. V. V., PIETERS, C. M. and SANDLIN, D. L. (1981): Particulate mineral mixtures: The rela-

tion of albedo and apparent absorption band strength. Lunar and Planetary Science XII. Houston, Lunar Planet. Inst., 547–549.

LOEFFLER, B. M., BURNS, R. G., TOSSELL, J. A., VAUGHAN, D. J. and JOHNSON, K. H. (1974): Charge transfer in lunar materials: Interpretation of ultraviolet-visible spectral properties of the moon. Proc. Lunar Sci. Conf. 5th, Vol. 3, 3007–3016.

MAO, H. K. and BELL, P. M. (1975): Crystal-field effects in spinel: Oxidation states of iron and chromium. Geochim. Cosmochim. Acta, **39**, 865–874.

MASON, B. (1963): The hypersthene achondrites. Am. Mus. Novit., **2155**, 1–13.

McCORD, T. B., CLARK, R. N., HAWKE, B. R., McFADDEN, L. A., OWENSBY, P. D., PIETERS, C. M. and ADAMS, J. B. (1981): Moon: Near-infrared spectral reflectance, a first good look. J. Geophys. Res., **86** (B11), 10883–10892.

McFADDEN, L. A. (1981): Near-earth asteroids: 1981 perspectives based on reflectance spectroscopy. Bull. Am. Astron. Soc., **13** (3), 718.

McFADDEN, L. A., GAFFEY, M. J. and TAKEDA, H. (1981): The layered crust model and the surface of Vesta (abstract). Papers Presented to the Sixth Symposium on Antarctic Meteorites, 19–20 February 1981. Tokyo, Natl Inst. Polar Res., 62–64.

PARKIN, K. M. and BURNS, R. G. (1980): High temperature crystal field spectra of transition metal-bearing minerals: Relevance to remote-sensed spectra of planetary surfaces. Proc. Lunar Planet. Conf. 11th, 731–755.

SINGER, R. B. (1981): Near-infrared spectral reflectance of mineral mixtures: Systematic combinations of pyroxenes, olivine, and iron oxides. J. Geophys. Res., **86** (B9), 7967–7982.

SINGER, R. B. and BLAKE, P. L. (1982): Effects of mineral grain size and physical particle size on spectral reflectance of basalts. Presented to Div. of Planet. Sci. A.A.S, October, 1982.

STUBICAN, V. S. and GRESKOVICH, C. (1975): Trivalent and divalent chromium ions in spinels. Geochim. Cosmochim. Acta, **39**, 875–881.

TAKEDA, H. (1979): A layered-crust model of a howardite parent body. Icarus, **40**, 455–470.

TAKEDA, H. and MORI H. (1981): Yamato-75032, a missing link between diogenites and eucrites (abstract). Meteoritics, **16** (4), 390–391.

TAKEDA, H., MIYAMOTO, M., YANAI, K. and HARAMURA, H. (1978): A preliminary mineralogical examination of the Yamato-74 achondrites. Mem. Natl Inst. Polar Res., Spec. Issue, **8**, 170–184.

TAKEDA, H., MIYAMOTO, M., ISHII, T., YANAI, K. and MATSUMOTO, Y. (1979): Mineralogical examination of the Yamato-75 achondrites and their layered crust model. Mem. Natl Inst. Polar Res., Spec. Issue, **12**, 82–108.

TAKEDA, H., MORI, H., YANAI, K. and SHIRAISHI, K. (1980): Mineralogical examination of the Allan Hills achondrites and their bearing on the parent bodies. Mem. Natl Inst. Polar Res., Spec. Issue, **17**, 119–144.

TAKEDA, H., MORI, H. and YANAI, K. (1981): Mineralogy of the Yamato diogenites as possible pieces of a single fall. Mem. Natl Inst. Polar Res., Spec. Issue, **20**, 81–99.

VENABLE, W. H., WEIDNER, V. R. and HSIA, J. J. (1976): Information sheet on optical properties of pressed Halon coatings, report. National Bureau of Standards, Washington, D. C.

(Received May 21, 1982; Revised manuscript received August 31, 1982)